Analytic Surface Reconstruction by Local Threshold Estimation in the Case of Simple Intensity Contrasts

Peter J. Yim*, Ronald M. Summers

Diagnostic Radiology Department, National Institutes of Health, Bethesda, MD. 20892

ABSTRACT

Surface reconstruction for 3D visualization requires both a segmentation of the image and at the least, a conversion of the data from an image format to a shape format. While the discrete pixel locations of the segmentation may be satisfactory for quantitative purposes, it is usually important for visual quality to remove such voxelation in the shape data prior to rendering. Removal of such voxelation, depending on the specific segmentation technique, may be problematic, involving excessive interpolation prior to segmentation or the application of pure surface smoothing in which important image information may be disregarded. An algorithm is presented here to address these problems. In this algorithm, a smoothly varying threshold level is determined such that that level falls within the interpolated intensity ranges of all the segmentation-boundary voxels. This threshold information is extrapolated to voxels adjacent to the boundary and then used to correct or normalize the original image in the vicinity of the boundary. Provided that the directionality of the contrast between the interior and exterior of the boundary is sufficiently consistent throughout the boundary, an isosurface of this normalized image is guaranteed to exist which falls within the voxels of the segmentation boundary.

Keywords: Surface reconstruction, Segmentation, Watershed, Marching-cubes algorithm, Surface aliasing, Interpolation

1. INTRODUCTION

Surface reconstruction, the localization and representation of the boundary from 3D images is akin but not equivalent to segmentation or the classification of points within the image. While the location of boundaries are implicit or sometimes explicit within a given segmentation method, conventionally, the sub-voxel location and complexity of the boundary are not. Thus, in the segmentation, with certain exceptions including the Marching-Cubes (MC) Algorithm[1] and the deformable-model class of segmentation[2], without further processing substantial pixelation or aliasing of the boundary will exist which presents serious problems for visualization, shape characterization for finite element analysis[3,4,5,6] for example and even conceivably volumetry[7] . Thus, in general, methods of surface-reconstruction are needed to accommodate the wide range of potential segmentation methods including watershed-based[8,9] clustering-based[10],[11] and even manual methods♣[12] still quite important for clinical and experimental purposes.

This problem has been previously described simply as an interpolation problem; that the surface derived from the segmentation will have adequate resolution provided the resolution of the image is sufficiently increased prior to the segmentation. Thus, in addition to the conventional interpolative methods[13], new methods which particularly address the large inter-slice dimension have been proposed[14,15,16]. However, this approach may be limited due to the dramatically increased memory requirements and computation time needed to achieve a sufficient increase in segmentation resolution.

* Correspondence: Email: pyim@fourier.cc.nih.gov

♣ The problem of surface reconstruction has encompassed the problem of the determination of the connectivity between 2D contours. This topic is not addressed in this paper.

Another common approach to surface reconstruction from segmentation is to simply perform a spatial smoothing of the literal segmentation boundary[17,18]. Such methods may produce visually or even quantitatively acceptable results but do not fully exploit the underlying image intensity information and generally cannot distinguish true roughness of the surface from surface aliasing.

Looking at this problem from a different point of view, very effective means of determining isosurfaces from image data have been developed which identify locations or vertices on the surface directly from the image data in an interpolative manner the most well-known technique of which is the MC algorithm[1] but in general the problem can be expressed as the solution to the equation[19]:

$$I(x, y, z) = T \tag{1}$$

Where $I(x,y,z)$ is the interpolation function of the image intensities and T is some constant threshold value. The application of this methodology in quantitative medical image analysis is limited, however, since the determination of a threshold value for the boundary of an object may be problematic and often no one threshold value is valid throughout the boundary of any given object due to a variety of artifacts of potential artifacts for MRI[20] in both and x-ray computed tomography[21]. Removal of such variability will be the essence of our methods presented here with a new emphasis placed on the correspondence between the resulting isosurface and a given segmentation.

Several methods have been proposed to directly remove variability or "inhomogeneity" from the image, particularly for MRI. Perhaps the most generic of these methods is that of Dawant[22] *et al* whereby points within various parts of the image known to be isointense (being of the same tissue type) are identified by the user. From that information a surface is fit which provides correction factors for the entire image. Various methods have subsequently been developed to provide greater automation which include a high-pass filtering method[23] and methods whereby the corrections are integrated with specific segmentation methods[24,25]. Once the intensity corrections have been applied to the image, in principle, threshold levels exist at which valid isosurfaces of the various tissue types can be constructed. Alternatively, this approach to surface reconstruction could be considered as a generalization of (1):

$$I(x, y, z) = T(x, y, z) \tag{2}$$

Where the threshold level, $T(x,y,z)$, is now a function of location.

In this paper, we present a new method of determining this threshold function within the vicinity of the segmentation boundaries which is consistent with any boundary independent of the segmentation method. This method has application on a relatively wide class of boundaries where there is uniform directionality of the intensity contrast along the boundary.

2. Formulation of the Problem

Segmentation methods which classify pixels or voxels into regions and/or boundary points are inherently ambiguous at the boundaries. In segmentation methods such as the watershed where a boundary of finite thickness is produced between adjacent regions, the exact location of the dividing line between two tissue types, for example, may fall anywhere within the finite thickness of the boundary. This problem is not avoided in segmentation methods where adjacent regions abut one another with no intervening boundary; this type of classification should be interpreted to mean that the classification of points along the boundary is *best* classification of the given point but that in reality points along the boundary are, to various extents, part of both regions.

The various types of boundaries formed from segmentation can be construed to be the range on a dividing line or dividing surface between the regions. This is most straightforward in the case of a 6-neighbor 3D boundary or a 4-neighbor 2D boundary as shown in figure 1(c). At the least, this segmentation boundary implies that the dividing line such as an isointensity line shown in figure 1(b) between the two regions falls within the finite thickness of that boundary region.

The situation is less well defined for boundary regions with lower connectivity such as for the 27-neighbor boundary in 3D or the 8-neighbor boundary in 2D which is shown in figure 1(d). In this case, not only should points within the boundary region be considered to be a mixture of the two adjacent regions but also some points *within* the classified regions adjacent to the boundary since in this case, some points within the classified regions are directly adjacent to points within the other classified region. Specification of the range over which the dividing line could be located in this case is more arbitrary in this case. Strictly speaking, two possibilities for determining the range or region of the boundary would be (a) all points within the boundary plus all points of either classified region which are adjacent to points in the adjacent classified region or (b) all points in the boundary plus some portion of the classified points which are immediately adjacent to the other classified region. However, a reasonable alternative which is used in our methods to be described later, is to simply ignore the incompleteness of the 27 or 8-neighbor boundary and consider that the boundary line must pass through all points in the boundary region but may also pass through points outside of the boundary region. Hopefully, once such constraint is placed on the dividing line, the location of the dividing line outside the boundary region would only be at intermediate points immediately adjacent to the boundary. A similar interpretation can be made of a segmentation where there is no explicit boundary such as is shown in figure 1(e).

Once a boundary of finite thickness has been defined based on the segmentation, a "variable-intensity" surface can be constructed so as to be confined to lie within the thickness of the segmentation boundary. As will be discussed in detail in the next section, the surface will generally fall within the segmentation boundary at a given point if the threshold function $T(x,y,z)$ at that point falls within the limits of the interpolation function $I(x,y,z)$ for the given boundary voxel. A method is presented which determines $T(x,y,z)$ which varies in the smoothest possible way along the boundary.

3. Algorithm

Determination of a threshold level which both falls within the intensity ranges of each boundary voxel and varies smoothly from one voxel to the next is relatively straightforward. First of all, the range for the discrete threshold function T_i within a given boundary voxel is between the minimum and maximum of the trilinear interpolation function $I(x,y,z)$ within the voxel:

$$\begin{aligned} T_{\min,i} &= Minimum(I(x+d_x, y+d_y, z+d_z)), \\ T_{\max,i} &= Maximum(I(x+d_x, y+d_y, z+d_z)), \\ -\tfrac{1}{2} < d_x, d_y, d_z &< \tfrac{1}{2} \end{aligned} \qquad (3)$$

Where (x,y,z) is the location at the center of the given boundary voxel or boundary face, i, for a segmentation without an explicit boundary region.
We have implemented a smoothing whereby the value of the threshold at each point ideally is the average of its immediate neighbors.

$$T_i = \frac{1}{n}\sum_{j=1}^{n} T_j \ , \ T_j \text{ is one of } n \text{ immediate neighbors of } T_i \ . \qquad (4)$$

This condition of the threshold levels is analogous to that of the vertical positions of point objects in a mechanical system at equilibrium in which the point-objects are constrained to move only in the vertical direction and are interconnected to their neighbors by springs which pull with a force proportional to their vertical displacement as shown in figure 2. If displaced from it's equilibrium position, the point objects in the system will experience a force proportional to the displacement of a given object from its current equilibrium position. Provided that the motion of the objects is sufficiently damped it will obey the differential equation:

$$\frac{dT_i}{dt} = K(T_{eq} - T_i) \tag{5}$$

$$T_{ave,i}, T_{\min,i} < T_{ave,i} < T_{\max,\, i}$$

$$T_{eq} = \{\ T_{\min,i}, T_{ave,i} < T_{\min,i}$$

$$T_{\max,\, i}, T_{\max,\, i} < T_{ave,i}$$

$$T_{ave,i} = \frac{1}{n} \sum_{j=1}^{n} T_j$$

The solution to this equation can be obtained numerically by finite differences:

$$\Delta T_i = K(T_{eq} - T_i)\Delta t = (K\Delta t)(T_{eq} - T_i) \tag{6}$$

In our implementation, the constant factor $K\Delta t$ was set to 0.25 and the calculation was performed for 10 iterations and the T_i 's were initialized to the mid-point of the intensity ranges of each voxel, $1/2(T_{max,i} + T_{min,i})$.

Two methods of extrapolation of the threshold level to adjacent voxels are:

(a) Once the threshold level was determined for each of the boundary points it was extended to neighboring voxels on a "nearest-neighbor" basis; all voxels with 6-neighbor adjacency to the boundary were assigned the threshold of the adjacent boundary voxel. Those new voxels are then considered part of the boundary and the process is repeated once more. This method was used for the cerebral ventricle surface reconstruction.

(b) The voxels 26-neighbor adjacent to the boundary have a threshold level which is a weighted average of the threshold levels of all it's neighbors within the boundary with the weight being the inverse of the distance. This method was used for the thoracic aorta surface reconstruction.

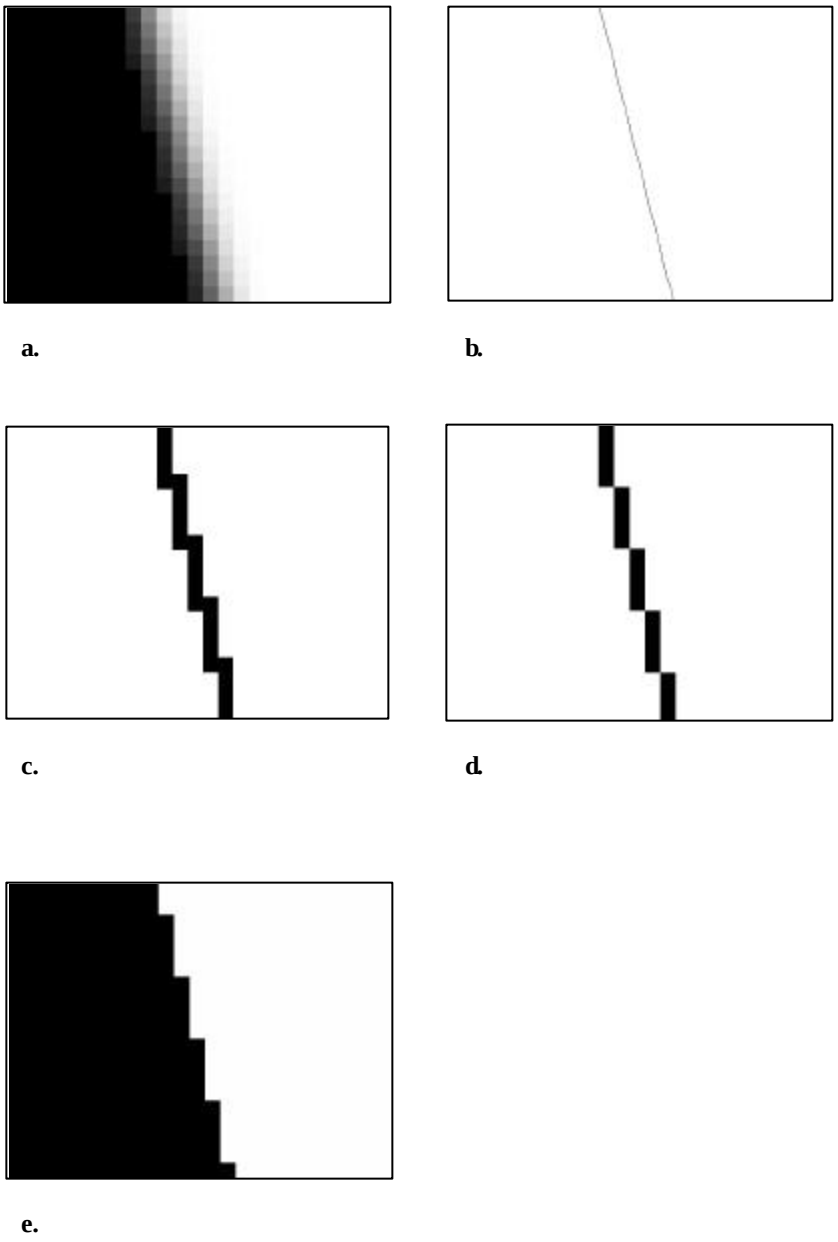

Figure 1. Types of segmentation boundaries. Classification-type segmentation of a given image may produce various types of boundaries. A test image of two regions is created at low resolution with the intensities along the boundary determined by the degree to which each pixel is occupied by each of the two regions. Then that image is blurred by a 2D gaussian with a space constant of 1 pixel unit with a cross section shown in (a). The cross-section of a MC isointensity surface is shown in (b). Various classification segmentation are shown including that of a 4-neighbor boundary (c) an 8-neighbor boundary (d) and without an explicit boundary (e).

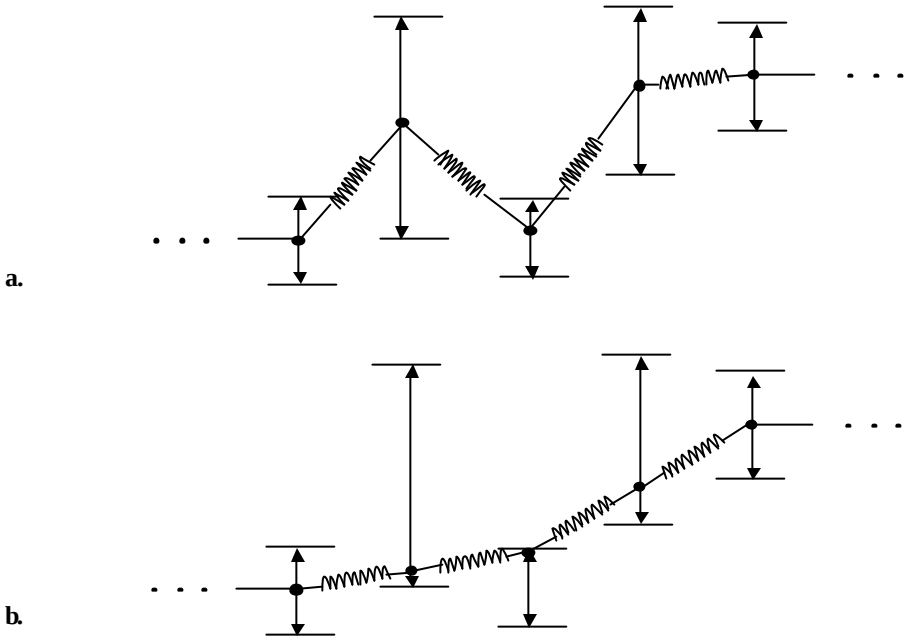

Figure 2. Mechanical analogy of threshold determination algorithm. The threshold value at each point on the segmentation boundary is an object which is constrained to move only in the vertical direction and within fixed limits, which are the maximum and minimum values of the interpolated image intensity within the bounds of the given voxel. Springs attach each points to its neighors (only two neighbors shown here for purposes of illustration) which pulls with a force proportional to their vertical displacement. The nodes are initialized to the midpoints of the intensity ranges (a) and move towards an equilibrium position (b).

3. Results

3.1 Test images

Test images were created of a cylinder and a sphere at low resolution with intensities at the boundaries of the cylinder proportional to the degree to which they were occupied by the cylinder to simulate the partial volume effect. That image is added to a ramp function whose contrast across the diameter of the object is 2/3 that of the cylinder/sphere-background contrast. The resulting cylindrical image is blurred with a 2D gaussian with a space constant of 1.0 voxels and the resulting sphere image is blurred with a 3D gaussian with a space constant of 1.0 voxels.. A cross section of cylinder image is shown in (a) and is comparable to the sphere image through its center. The image was then segmented with the Interactive Meyer Watershed whose boundary has 26-neighbor connectivity, initialized by one point at the center of the cylinder and one distant from the cylinder.

The segmentation boundaries of the cylinder and the sphere image were the same for the center slice and was symmetric but highly pixelated as shown in figure 3. The variable-intensity surface reconstructions are good approximations to the circular shape from which the images were generated. For the surface reconstruction from the image of the cylinder, the cross-section of the reconstructed surface is slightly "squared" with the "corners" of the reconstructed cross-section at almost the same location as that of the true circular cross-section while the "sides" of the reconstructed cross-section are displaced inwards by about 1/3 voxel. On the other hand, the cross-section of the surface reconstruction of the image of the sphere has extremely little distortion although it is uniformly displaced inwards by about 1/4 voxel from the true location.

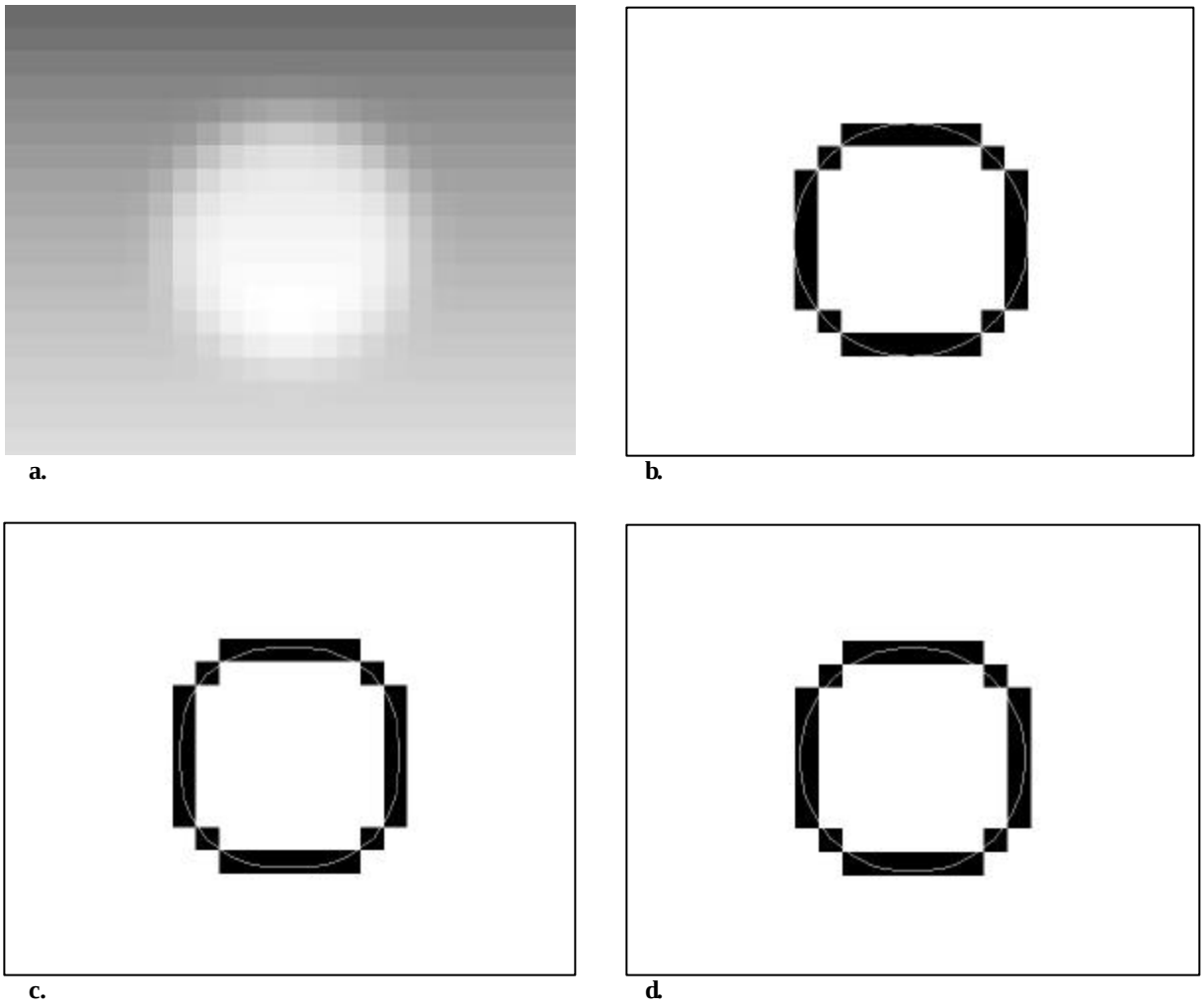

Figure 3. Performance of surface reconstruction on test image. A test image was created of a cylinder and a sphere at low resolution with a intensities at the boundaries of the cylinder/sphere proportional to the degree to which they were occupied by the cylinder/sphere to simulate the partial volume effect. That image added to a ramp function varying in the vertical direction and then blurred by convolution with a gaussian of space constant 1.0 voxels (2D blurring for cylinder image, 3D gaussian blurring for sphere image). A cross section of the cylinder image is shown in (a) which is comparable to that of the midsection of the sphere image. The image was then segmented with the interactive Meyer Watershed initialized by one point at the center of the cylinder and one distant from the cylinder/sphere. The segmentation boundary at the mid-section was the same for both images and is shown as the black pixels in (b) with the boundary of the cylinder/sphere from which the image was derived shown as the white trace. The variable-intensity surface reconstruction for the cylinder and the sphere image are shown in (c) and (d) respectively.

3.2 Thoracic aorta

An image of the lumen of the thoracic aorta obtained by contrast-enhanced magnetic resonance angiography in a patient with familial hypercholesteremia[26] with 2-mm thick 50%-overlapping slices in a 256x160 matrix in a 28-cm field of view, zero-fill interpolated out-of-plane 2x and in-plane to 256x256 dimension. The image was segmented by the Interactive Meyer Watershed with 26-neighbor boundary connectivity with 6x6x2 markers placed about a point at the center of the aorta and a point distant from the aorta representing respectively the interior and exterior of the aorta. The entire aorta within the field of view was correctly classified while segmentation of the branches of the aorta was somewhat variable. A 150x256x60 region of the image was processed on the SGI octane (195 MHz) requiring 4 minutes for the watershed segmentation, 26 seconds for the image normalization, 44 seconds for the Marching Cubes isosurface reconstruction and 34 seconds for the initial surface rendering.

a. **b.**

Figure 4. Surface reconstruction of magnetic resonance angiogram of aorta. Meyer watershed initialized with square patches indicating the interior and exterior of the vessel. Cropped version of original image shown in maximum intensity projection (MIP) form is shown in (a) with watershed initializations shown as high intensity regions. Results of variable-intensity surface reconstruction shown in (b).

Segmentation and surface reconstruction was preceded by convolution of the image with a gaussian of space constant 1.0 to minimize the effects of image noise. The 3D surface is shown in figure 4.

3.3 Cerebral ventricles

One sample cerebral MR image from a brain study was used for testing as acquired and segmented into grey-matter, white matter and cerebral spinal fluid (CSF) as described in ref. [10]. In this case no explicit boundary region is produced by the segmentation but boundary "voxels" were considered to 1/2 of the voxel to either side of a face of the boundary with the interpolated intensity ranges determined accordingly and the adjacency of the points was determined from that of the boundary faces. The image was smoothed by convolution with a gaussian of space constant 1.0 prior to the surface reconstruction. Normalization of the image required 2 minutes 25 seconds, the Marching Cubes isosurface reconstruction required 3 seconds and the initial surface rendering required 8 seconds all on the SGI Onyx Workstation which primarily differs from the Octane workstation (used for the aortic reconstruction) for these purposes only in its greater memory size.

a.

b.

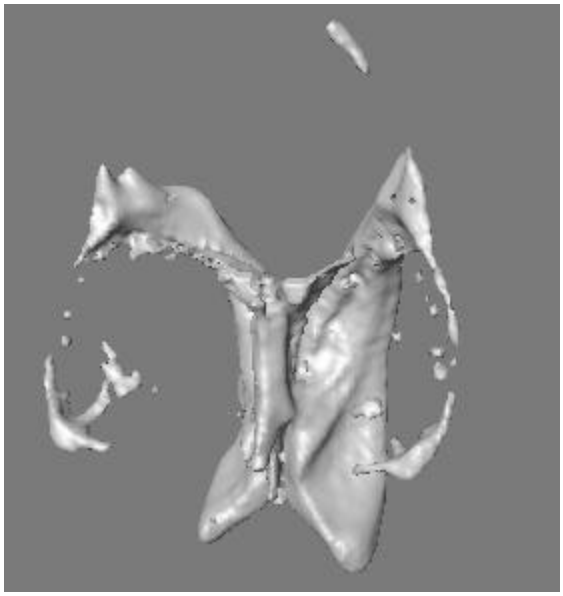

c.

Figure 5. Surface reconstruction of ventricles of brain. Surface reconstruction method applied to brain images (c) acquired and segmented as in ref [10] with representative slice shown in (a) and segmentation of that slice shown in (b) with the ventricular region indicated by the arrow.

4. Discussion

4.1 Completeness of surface

The methods described above do not guarantee that a closed surface will be produced for any segmentation of a given object in any given image. Rather, this method is restricted to cases where the directionality of the contrast between the interior and exterior of the object is generally uniform throughout the boundary of the object; *ie.* voxels on the interior of the boundary are high relative to adjacent voxels on the exterior side of the boundary or *vice versa*. The exact conditions for production of the isosurface at any given point in the boundary are slightly more complicated as will be discussed below.

Consider the formulation of the surface based on a boundary of single-voxel thickness with six-neighbor connectivity as in figure 1. The condition for the existence of a closed isosurface which falls completely within the thickness of that type of boundary is that no continuous path through the interpolated image intensities penetrates the boundary which is either entirely above or below the isosurface intensity value. Several possible configurations of boundary intensities are shown in figure 6 where three cases are shown including the case where the surface will definitely have no holes or leaks, where the surface will definitely have a leak and a third case where additional information is required to make the determination, all assuming trilinear interpolation. The MC algorithm itself is not guaranteed to produce the correct results for the third case but subsequent research has provided methods for doing so.[16, 27,28]

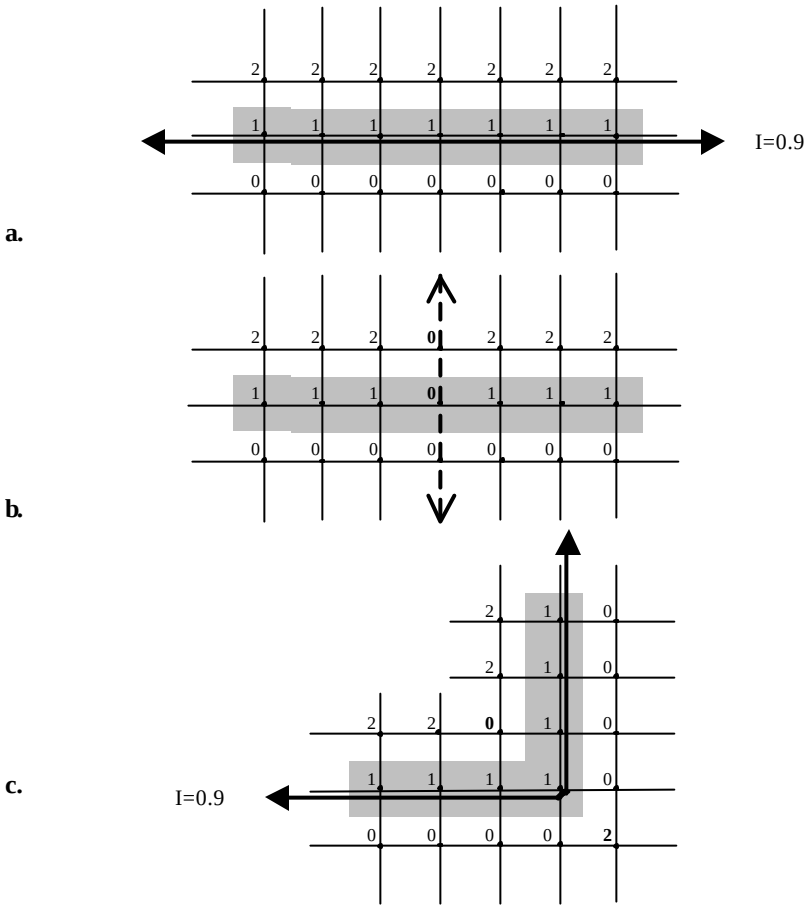

Figure 6. Conditions for the successful generation of a closed surface from the segmentation-boundary normalization method. In (a) the boundary pixels (shown as the dark region) are clearly separate a high from a low intensity regions. In (b) there is clearly a gap in the boundary. In (c) there is a reversal in intensities in the boundary but is moderate enough not to cause a gap in the boundary.

4.2 Accuracy of threshold determination

Given N estimates of a threshold intensity expressed in terms of intensity ranges, and assuming, for simplicity, that those ranges are all of equal size, the degree of overlap of those intensity ranges and thus the precision of the cumulative estimate of the threshold intensity are statistical in nature. Symbolically, for the set of points, P each with an intensity range $T_{min,i}$ to $T_{max,i}$:

$$\forall i \in P, T_{\min,i} < T < T_{\max,i} \tag{7}$$

and the size of the intensity range, R is given by:

$$R = T_{\max,i} - T_{\min,i} \tag{8}$$

For each of the N points, the intensity range has a random offset from the true threshold level in the range of 0 to R_i.

$$T = T_{\max,i} - d_i, \qquad 0 < d_i < R \tag{9}$$

and percentage-wise, the size of the overlap of the intensity ranges of any two points is:

$$S = 1 - |d_i - d_j| / R \tag{10}$$

So, for example, for an overlap of 10% or less between two points:

$$0.9R \leq |d_i - d_j|, \qquad d_i > d_j \tag{11}$$

which is shown graphically in figure 7(a) which will occur only 1% of the time as is calculated as a ratio of areas in the graph. Determination of the occurrence rate of such an overlap size amongst a greater number of points is more complex but a conservative estimate can be made. Rather than the specification of (11) assume that the following criteria must be true to produce a 10% overlap:

$$\begin{aligned} &0.05R > d_i \quad \textit{and} \quad 0.95R < d_j \quad \textit{or} \\ &0.05R > d_j \quad \textit{and} \quad 0.95R < d_i \end{aligned} \tag{12}$$

which is described in the graph of figure 7(b) and gives a conservative estimate of the probability. Usefully, this description lends itself to a determination of the probability of a given overlap for N points.

Consider first what is the probability that δ of at least one of the N points is less than 0.05R. That probability is just the complement of the probability of *none* of the points having δ less than 0.05 which is given directly by the binomial distribution. If the probability of δ less than 0.05 for a single point is p and the variable representing the number of points with δ less than 0.05 is X:

$$\Pr ob(X \geq 1) = 1 - \Pr ob(X = 0) = 1 - (1-p)^N = 1 - 0.95^N \tag{13}$$

Given that the probability is the same for the outcome Y, of at least one point with δ greater than 0.95 and assuming that the outcomes X and Y are relatively independent, the combined probability is given by:

$$\Pr ob(Y \geq 1 \mid X \geq 1) \Pr ob(x \geq 1) \approx \Pr ob(Y \geq 1) \Pr ob(X \geq 1) = (1 - 0.95^N)^2 \tag{14}$$

For N=60, this probability is 0.91. In other words, given 60 points estimating a threshold level, there is at least a 91% chance that the overlap or the precision of the threshold estimation will be less than 10% of the intensity range R.

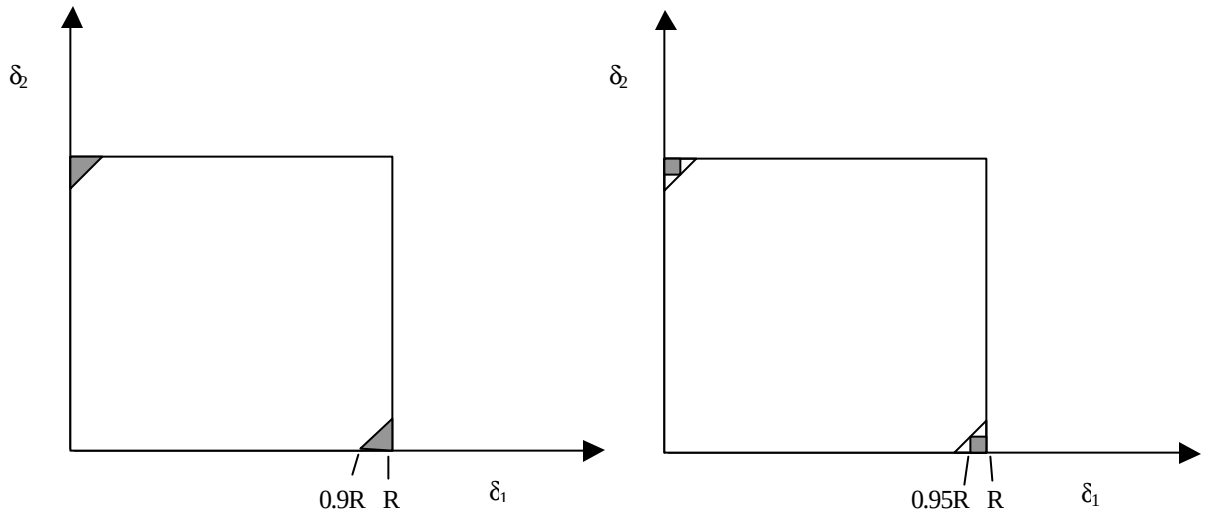

a. **b.**

Figure 7. Probability of less than 10% overlap between two intensity ranges of size R, offset from a common point by δ_1 and δ_2 respectively, which range, with uniform probability, from 0 to R . Less than 10% overlap between the two intensity ranges is equivalent to the condition: $|\delta_1 - \delta_2| > 0.9R$ which is true for the darkened region in (a) which in this case is a 1% probability. A conservative approximation to this condition which will allow for calculations for multiple intensity ranges, is for both $\delta_1 < 0.05R$ *and* $\delta_2 > 0.95R$ or *vice versa* which is true for the darkened region in (b) which is a 0.5% probability.

5. Conclusions

In many cases, problems of segmentation, regarding the classification of whole voxels in the image, overwhelm the surface-reconstruction problem which generally relates to the sub-voxel resolution of the boundaries. However, such surface reconstruction may be important for both the qualitative and quantitative interpretation of an image. In this paper we formulated the surface-reconstruction problem as a process independent of segmentation; whereas the segmentation process produces approximate boundaries at the resolution of the voxel size, the surface-reconstruction is concerned with the exact localization of the surface. We have proposed here a method which under relatively simple conditions of the interior-exterior contrast is entirely derived from and compatible with the segmentation.

Acknowledgments

We would like to thank Dr. Goldszal, a member of our department, for providing the cerebral MRI's, segmentations and the necessary explanations.

6. REFERENCES

1. WE Lorensen and HE Cline, "Marching Cubes A high resolution 3-D surface construction algorithm," *Computer Graphics*, 21(4):163-169, 1987.
2. T McInerney and D Terzopoulos, "Deformable models in medical image analysis: a survey," *Medical Image Analysis*, 1(2):91-108, 1996.
3. DLA Camacho, RH Hopper, GM Lin, and BS Myers, "An improved method for finite element mesh generation of geometricaly complex structures with application to the skullbase," *J Biomech*, 30(10): 1067-1070, 1997.
4. D Ulrich, B van Rietbergen, H Weinans, and P Ruegsegger, "Finite element analysis of trabecular bone structure: a comparison of image-based meshing techniques," *J Biomech*, 31(12): 1187-1192, 1998.
5. P Cahoon and A Hannan, "An interactive modelling environment for craniofacial reconstruction," *Proceedings of SPIE*, 2178:206-215, 1994
6. JA Moore, DA Steinman, DW Holdsworth, CR Ethier, "Accuracy of computational hemodynamics in complex arterial geometries reconstructed from magnetic resonance imaging," *Ann Biomed Eng*, 27: 32-41, 1999.
7. T Kaneko and Y Yamamoto, "Volume-preserving surface reconstruction from volume data," *Proceedings, International Conference on Image Processing*, 1: 145-148, 1997.
8. F Meyer and S Beucher. "Morphological Segmentation," *Journal of Visual Communication and Image Representation*, 1(1):21-46, 1990.
9. PJ Yim, D. Kim, and C Lucas, "High Resolution Four-dimensional surface reconstruction of the right heart and pulmonary arteries," *Proceedings of SPIE*, 3338: 726-738, 1998.
10. AF Goldszal, C Davatzikos, DL Pham, MXH Yan, RN Bryan and SM Resnick, "An image-processing system for qualitative and quantitative volumetric analysis of brain images," *J Comput Assist Tomogr*, 22(5):827-837, 1998.
11. JC Bezdek, LO Hall, LP Clarke, "Review of MR image segmentation techniques using pattern recognition," *Med Phys*, 20:1033-48, 1993.
12. AL Reiss, F Faruque, S. Naidu et al, "Neuroanatomy of Rett Syndrome: a volumetric imaging study," *Ann Neurol*, 34: 227-234, 1993.
13. GJ Grevera and JK Udupa, "An objective comparison of 3-D image interpolation methods," *IEEE Trans Med Imaging*, 17(4), 642-652, 1998.
14. SP Raya and JK Udupa, "Shape-based interpolation of multidimensional objects," *IEEE Trans Med Imaging* , 9: 32-42, 1990.
15. WE Higgins, C Morice and EL Ritman, "Shape-based interpolation of tree-like structures in three-dimensional images," *IEEE Trans Med Imaging*, 12:439-450, 1993.
16. DT Puff, D Eberly, and SM Pizer, "Object-based interpolation via cores," *Proceedings of SPIE*, 2167: 143-150, 1994.
17. G Taubin, "A signal processing approach to fair surface design," *Computer Graphics Proceedings, Siggraph*, 351, 1995.
18. DF Watson, *Contouring. A Guide to the Analysis and Display of Spatial Data*, Pergamon Press, Oxford, 1992.
19. P Ning and J Bloomenthal, "An evaluation of implicit surface tilers," *IEEE Computer Graphics and Applications*, pp. 33-41, 1993.
20. RR Edelman and JR Hesselink, eds. *MRI; Clinical Magnetic Resonance Imaging*, W.B. Saunders Company, 1990.
21. TT Thompson, *A Practical Approach to Modern Imaging Equipment*, Little Brown and Company, Boston, 1985.
22. BM Dawant, AP Zijdenbos and RA Margolin, "Correction of intensity variations in MR images for computer-aided tissue classification," *IEEE Trans Med Imaging*, 12(4):770-781, 1993.
23. B Johnston, MS Atkins, B Mackiewich and M Anderson, "Segmentation of multiple sclerosis lesions in intensity corrected multispectral MRI," *IEEE Trans Med Imaging*, 15(2):154-169, 1996.
24. DL Pham, JL Prince, "An adaptive fuzzy c-means algorithm for image segmentation in the presence of intensity inhomogeneities," *Proceedings of SPIE*, 3338:555-563, 1998.
25. WM Wells, WEL Grimson, R Kikinis, and FA Jolesz, "Adaptive segmentation of MRI data," *IEEE Trans Med Imaging*, 15(4):429-442, 1996.
26. RM Summers, LM Pusanik, JD Malley, JM Hoeg, "Fractal analysis of virtual endoscopy reconstructions," *Proceedings of SPIE*, (In press)
27. BK Natarajan, "On generating topologically correct isosurfaces from uniform samples," *Hewlett-Packard Laboratories Technical Report HPL-91-76*, Hewlett-Packard, Palo Alto, Calif., 1991.
28. GM Nielson and B Hamann, "The asymptotic decider: resolving the ambiguity in marching cubes," *Proceedings of IEEE Visualization 91*, 81-91, 1991.